

Optical response in one-dimensional Mott insulators

S. S. Kancharla and C. J. Bolech

Serin Physics Laboratory, Rutgers University, Piscataway, New Jersey 08854-8019

(Received 8 May 2001; published 8 August 2001)

We study the optical response of a Mott Hubbard system in the framework of the half-filled extended Hubbard model using the density matrix renormalization group (DMRG) method. We discuss the appearance of excitonic features inside the spectral gap as the system goes from the spin density wave (SDW) to the charge density wave (CDW) phase.

DOI: 10.1103/PhysRevB.64.085119

PACS number(s): 71.10.-w, 71.35.-y, 72.80.Sk, 78.30.Am

A detailed understanding of the optical response and charge gap in the one-dimensional Mott insulators remains a challenge to existing theoretical methods. Renewed interest in the subject stems from several experiments on materials such as SrCuO₂, Sr₂CuO₃, conjugated polymers and Ni halides¹⁻³ with possible applications such as ultrafast switching in optoelectronic devices. The aim of this letter is to study the effect of nearest neighbor Coulomb repulsion on the optical and Raman spectrum in these systems.

A simplified model which has been used to describe the essential physics of these materials is the extended Hubbard model (EHM) defined as

$$H = -t \sum_{j,\sigma} (c_{j+1,\sigma}^\dagger c_{j,\sigma} + \text{H.c.}) + U \sum_j \left(n_{j\uparrow} - \frac{1}{2} \right) \left(n_{j\downarrow} - \frac{1}{2} \right) + V \sum_j (n_j - 1)(n_{j+1} - 1). \quad (1)$$

The first term corresponding to hopping between nearest neighbor sites and the second term to the onsite Coulomb repulsion provide the competition between itineracy and localization in the regular Hubbard model. The third term represents Coulomb repulsion between electrons occupying nearest neighbor sites. The Hamiltonian as written above guarantees an insulating ground state with a filling of one electron per site.

Although this model has been widely studied, many questions remain unanswered. The analytic approach at its best in Bethe-ansatz provides an exact solution only when $V=0$.⁴ The method has been used to obtain the energy spectrum and thermodynamics, but a reliable computation of dynamical quantities such as the optical response remains elusive. Non-perturbative analytic studies of the dynamical response in these systems have largely been constrained to use the continuum limit.⁵

Numerical methods such as exact diagonalization, although valuable in providing real frequency information, are limited to small system sizes.⁶ Quantum Monte Carlo methods can treat large finite size clusters but analytic continuation from imaginary to real frequencies is an unreliable procedure.

The renormalization group idea has helped deal with some of the toughest problems in physics characterized by large number of degrees of freedom playing an essential role. The efficacy of the idea as a tool to compute experimentally

relevant quantities lies in the ability to integrate out the non essential degrees of freedom. This has been brought to fruition with tremendous success in a numerical algorithm for low dimensional interacting systems known as the density matrix renormalization group (DMRG).⁷ The numerical solution of finite size systems on a computer is restricted by an exponentially increasing Hilbert space. The DMRG method works around this by a systematic truncation. It prescribes how to retain the most probable states of a subsystem required for an accurate description of a particular set of states (usually, just the ground state) of the full system. The DMRG algorithm initially suited to deal only with ground state properties, was subsequently extended to compute dynamical correlation functions.^{8,9} One of the approaches known as the ‘‘Lanczos vector method’’ constitutes choosing the particular set above as the ground state plus a set of Lanczos vectors. The vectors are chosen to approximate the reduced Hilbert space of excited states which connect to the ground state via the operator whose correlation function is desired. This method is very efficient in capturing low energy sharp features such as excitons in the optical spectrum; especially when bulk of the weight is in a single peak. Excitonic features in multi particle correlation functions have been observed in the EHM in previous studies.^{10,11}

The EHM at half-filling shows an interesting phase diagram. In the weak coupling limit ($U \ll t$) the system undergoes a second order transition from a spin density wave (SDW) phase to a charge density wave (CDW) state as a function of increasing V , at $V = U/2 + \delta(U)$. For intermediate values of U the SDW and CDW phases are separated by a narrow region with a bond charge density wave (BCDW) order. As one approaches strong coupling ($U \gg t$), the transition is again from an SDW to a CDW phase at $V = U/2 + \delta(U)$, but it is now first order. The small correction $\delta(U)$ is positive and approaches zero at both the weak and strong coupling ends. The precise location of a tricritical point at the crossover between the first and second order transitions has been a subject of much investigation¹²⁻¹⁶ and is complicated by the existence of the BCDW order.

In our study we compute the optical response and local spectral function of the EHM in the strong coupling regime. We fix U at a realistic value of $12t$. The first order transition between the SDW and CDW phases is manifest in the optical properties as well as in the ground state energy. The relevant values of V for SrCuO₂ and Ni halides are in the SDW phase. All the results presented in this letter were obtained from

computations performed with finite size chains of $N_s=50$ sites with open boundary conditions using the Lanczos vector method. Studying other sizes ($N_s=18,34,66$) shows that results for $N_s=50$ are generic. We use the finite size version of the DMRG algorithm and choose $m=150$ for the largest sizes. Selected runs performed with higher values of m did not introduce significant changes in the results. Typical discarded weights were $O(10^{-6})$. To validate our code we compare our results for the static and dynamic properties with exact diagonalization for short chains.

We use the following definition for the response function:

$$\chi_{AB}(\omega) = \frac{i}{L} \int_0^\infty dt e^{i(\omega+i\epsilon)t} \langle 0 | [A^\dagger(t), B(0)] | 0 \rangle. \quad (2)$$

The real part of the optical conductivity is defined through the imaginary part of the current-current response with $\epsilon \rightarrow 0$,

$$\sigma'(\omega) = \frac{1}{\omega} \chi''_{jj}(\omega), \quad (3)$$

where

$$j = -it \sum_{j,\sigma} (c_{j+1\sigma}^\dagger c_{j\sigma} - c_{j\sigma}^\dagger c_{j+1\sigma}) \quad (4)$$

is the paramagnetic current operator. The non-resonant Raman spectrum in a Mott-Hubbard system is given by the response function of the stress energy tensor,¹⁷

$$\tau = -t \sum_{j,\sigma} (c_{j+1\sigma}^\dagger c_{j\sigma} + c_{j\sigma}^\dagger c_{j+1\sigma}). \quad (5)$$

In the case of an insulator $\chi_{\tau\tau}$ is not the dominant contribution to the total Raman spectrum. But it is interesting for a comparison with χ_{jj} because, j and τ are respectively odd and even under parity conjugation, apart from an overall phase.

In Fig. 1 we show the local spectral function for various values of V ranging from 0 to $9t$. In the SDW phase, the single particle gap (Δ_s) stays constant until a threshold value of V around $3t$ is reached and then starts reducing (cf. Fig. 4). Here and further in this letter when we refer to the gap in a correlation function we measure the position of the lowest energy peak. We ignore the tail part which comes about due to the small finite broadening that is used to represent the Lanczos continued fraction. This implies that our values for the gaps are tight upper bounds to the actual ones. At the SDW-CDW transition the spectral gap reduces abruptly reaching a finite value, jumps up and then starts increasing again in the CDW phase. Note that in the CDW phase, the site on which we compute the spectral function is empty in the ground state.

In Fig. 2 we report the current-current and nonresonant Raman response functions in the left and right columns, respectively. A systematic change in the optical response in the odd (χ_{jj}) and even ($\chi_{\tau\tau}$) channels is discernible as we sweep through V across the SDW and into the CDW phase. For $V=0$ we see a broad feature centered at around U , in

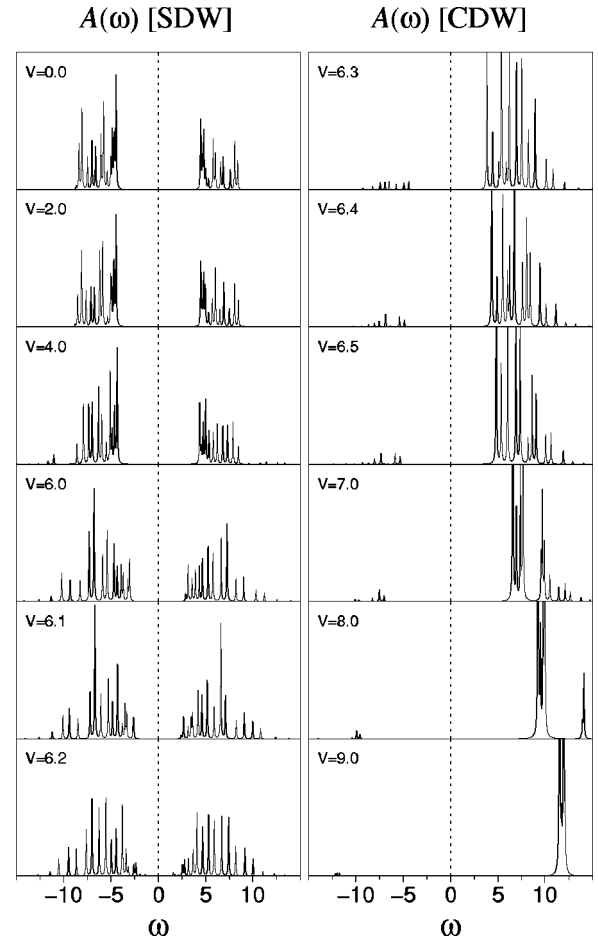


FIG. 1. Local spectral functions for different values of the coupling V . Note the abrupt change in particle-hole symmetry between the two phases.

good agreement with a recent calculation for the standard Hubbard model within the DMRG approach.¹⁸ Our method does not allow a resolution of the tiny bump seen in the middle of the broad optical absorption band. But, as V is increased we do notice the formation of a resonance which gradually gains in weight and shifts towards lower frequencies.^{11,19} This constitutes a precursor of the excitonic feature that we describe further below.

For small values of V the optical (Δ_{jj}) and Raman ($\Delta_{\tau\tau}$) gaps would be expected to coincide with the spectral gap, Δ_s . We find them to be slightly larger because it is not possible to create fully noninteracting electron-hole pairs in a finite size chain. Around $V \sim 1.5t$, the optical gap falls below the spectral gap in agreement with previous work.¹⁰ The same happens for the Raman gap at $V \sim 3t$. We define a quantity that we will call the excitonic weight ($W_{jj(\tau\tau)}$) as the fraction of the weight in the optical (Raman) spectrum below Δ_s ,

$$W_{jj(\tau\tau)} = \frac{\int_0^{\Delta_s} d\omega \chi_{jj(\tau\tau)}(\omega)}{\int_0^\infty d\omega \chi_{jj(\tau\tau)}(\omega)}. \quad (6)$$

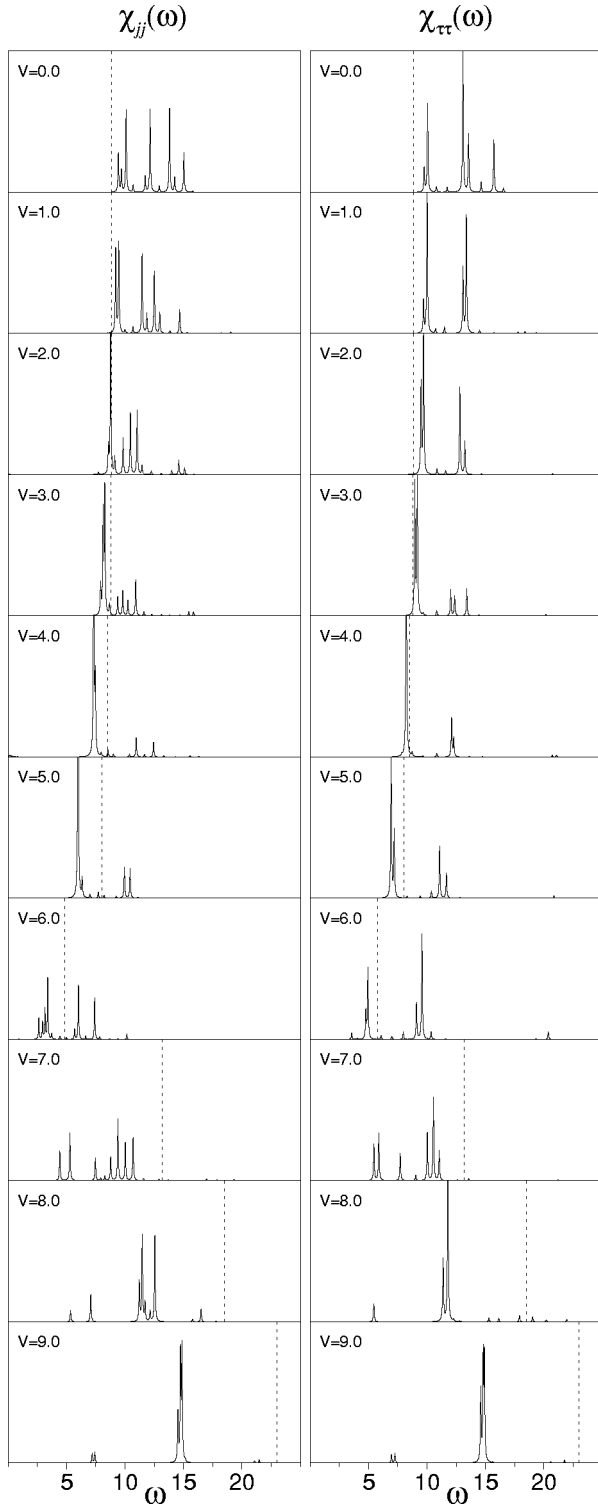


FIG. 2. Optical and Raman response functions for different values of the coupling V . The vertical dotted line indicates the magnitude of the single-particle spectral gap in each case.

In Fig. 3 we plot the excitonic weight as a function of V . In the case of both response functions it is seen that the excitonic weight is zero until the above mentioned crossing of gaps occurs (cf. Fig. 4). As V is increased further, the excitonic weight starts appearing and a resonance begins separat-

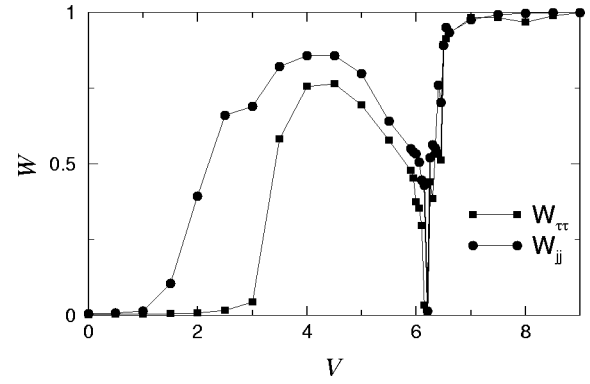


FIG. 3. Excitonic weight as a function of the coupling V .

ing from the rest of the spectrum. When $W_{jj(\tau\tau)}$ reaches a maximum around $V \sim 4t$, the spectrum is dominated by a sharp excitonic feature carrying most of the weight –86% (77%). This peak, well differentiated from the rest of the spectrum, is clearly located inside the single-particle spectral gap while the rest of the weight falls outside. The Lanczos method is rather well suited to describe these excitonic features, but it is not so good in capturing detail at the higher end of the spectrum. The optical bands inside the one-particle continuum tend to be shifted towards higher energies. At the same time the relative weight in the excitonic features is accurately represented, since we find that the sum rule for the optical conductivity in terms of kinetic energy is obeyed with 1% accuracy or better (except very close to the transition). As V is increased further beyond $V \sim 4t$ the excitonic feature starts losing weight and at the same time marches towards zero frequency. At the precise point of the SDW-CDW transition the excitonic mode reaches the lowest frequencies we can resolve ($\omega \sim 1/L$).

In a Mott insulator represented by the half-filled Hubbard model, creation of an independent electron-hole pair (or a holon-antiholon pair in the Bethe ansatz language) has a finite energy threshold; namely the spectral gap. This threshold is lowered in the presence of an attractive force by the binding energy of an electron-hole pair called an exciton. This attraction comes about due to the increased range of Coulomb repulsion in the EHM and is significantly absent in the standard Hubbard model. As we increase V the energy gained in binding electron-hole pairs keeps growing continu-

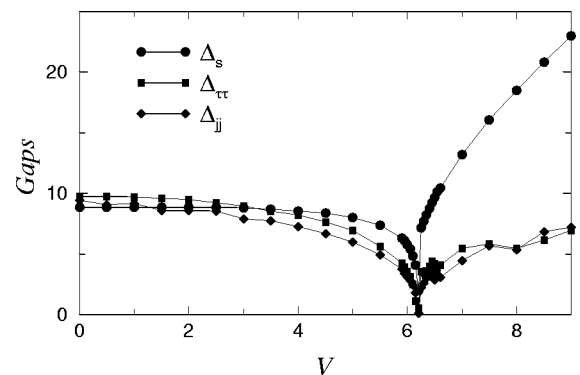


FIG. 4. Gaps for different values of the coupling V .

ously and the excitonic feature moves closer and closer to zero frequency. At the same time the density of electron and hole states available for binding first increases, reaches a maximum and then goes to zero at the SDW-CDW boundary. When the energy gained from binding the electron-hole pairs equals the energy cost of creating them across the single particle gap, the optical gap vanishes in both the odd (χ_{jj}) and even ($\chi_{\tau\tau}$) channels.

Amongst the examples of 1D Mott insulators mentioned earlier, we focus on Sr_2CuO_3 to indicate the experimental relevance of our results. From previous literature,^{20,21} the values of the parameters for this material are estimated to be: $t \approx 0.55\text{--}0.6$ eV, $U \approx 7.2$ eV and $V \approx 0.8$ eV. Therefore the material lies right near the boundary where excitonic weight in χ_{jj} begins to appear. Nevertheless, the exciton or its precursor in the form of a narrow peak distinguished from the rest of the spectrum should already be seen in the optical conductivity.

Although our interest is in the strong coupling limit one can gain an understanding of the physics at hand by using the language of the continuum limit applied to the EHM;¹⁴ an approach which is strictly valid only in the weak coupling case. Further using bosonization, the model can be split up into two sine Gordon models (SGM) for the charge and spin sectors, respectively. The charge sector is the only one of interest as far as (χ_{jj}) is concerned. On the other hand, spin-charge separation does not help a study of ($\chi_{\tau\tau}$) because the operator τ involves both the charge and spin sectors. The exact solution of the SGM is available and the spectrum is governed by a coupling parameter usually called β .²² For $\beta^2 < 4\pi$ the spectrum is built solely of kinks and antikinks.

As β increases further, the SGM enters the attractive regime and kink-antikink bound states known as breathers are formed. These bound states in the SGM correspond to the excitons in the EHM that form as the value of V is increased. Given that we are interested in the strong coupling regime of the EHM, a quantitative comparison with the attractive regime of the SGM falls beyond the margin of applicability of the scaling limit.

To conclude, we have shown that sharp excitonic features dominate the transport behavior in a particular regime of the EHM at half-filling. This is a direct consequence of the inclusion of nonlocal Coulomb interaction in this model. These excitons are of fundamentally different origin as compared to those in semiconductors formed by the binding of electron-hole pairs. Due to strong correlation and low dimensionality, electrons decouple into new elementary excitations, namely, spinons and holons. This necessitates a careful treatment of the full many-body problem. The Lanczos method combined with the DMRG approach is a powerful nonperturbative tool for computing the dynamical correlation functions of a non-trivial system like this. Our numerical approach permits us to easily include other ingredients such as explicit dimerization and interchain hopping which are present in these materials in order to allow a better quantitative comparison with experiments in the future.

We are indebted to G. Kotliar for several suggestions and to A. Rosch for his keen interest and many comments. We acknowledge useful discussions with N. Andrei, A. Millis, and S. Shastry. We thank K. Hallberg and S.R. White for discussions on the DMRG method.

-
- ¹Y. Mizuno, K. Tsutsui, T. Tohyama, and S. Maekawa, *Phys. Rev. B* **62**, R4769 (2000).
- ²*Conjugated Conducting Polymers*, edited by H. Kiess (Springer-Verlag, Berlin, 1992).
- ³H. Kishida, H. Matsuzaki, H. Okamoto, T. Manabe, M. Yamashita, Y. Taguchi, and Y. Tokura, *Nature (London)* **405**, 929 (2000).
- ⁴E.L. Lieb and F.Y. Wu, *Phys. Rev. Lett.* **20**, 1445 (1968).
- ⁵D. Controzzi, F.H.L. Essler, and A.M. Tsvelik, arXiv:cond-mat/0005349 (unpublished).
- ⁶R.M. Fye, M.J. Martins, D.J. Scalapino, J. Wagner, and W. Hanke, *Phys. Rev. B* **44**, 6909 (1991).
- ⁷S.R. White, *Phys. Rev. Lett.* **69**, 2963 (1992); *Phys. Rev. B* **48**, 10345 (1993).
- ⁸K.A. Hallberg, *Phys. Rev. B* **52**, 9827 (1995).
- ⁹T.D. Kuhner and S.R. White, *Phys. Rev. B* **60**, 335 (1999).
- ¹⁰W. Stephan and K. Penc, *Phys. Rev. B* **54**, R17269 (1996).
- ¹¹E.R. Chalbaud and J-P. Gallinar, *J. Phys.: Condens. Matter* **1**, 3325 (1989); J-P. Gallinar, *Phys. Rev. B* **48**, 5013 (1993).
- ¹²J.E. Hirsch, *Phys. Rev. Lett.* **53**, 2327 (1984).
- ¹³J.L. Cannon, R.T. Scalettar, and E. Fradkin, *Phys. Rev. B* **44**, 5995 (1991).
- ¹⁴J. Voit, *Phys. Rev. B* **45**, 4027 (1992).
- ¹⁵G.P. Zhang, *Phys. Rev. B* **56**, 9189 (1997).
- ¹⁶M. Nakamura, *Phys. Rev. B* **61**, 16377 (2000).
- ¹⁷B.S. Shastry and B.I. Shraiman, *Phys. Rev. Lett.* **65**, 1068 (1990).
- ¹⁸E. Jeckelmann, F. Gebhard, and F.H.L. Essler, *Phys. Rev. Lett.* **85**, 3910 (2000).
- ¹⁹F. Gebhard, K. Bott, M. Scheidler, P. Thomas, and S.W. Koch, *Philos. Mag. B* **75**, 47 (1997).
- ²⁰C. Kim, A.Y. Matsuura, Z.X. Shen, N. Motoyama, H. Eisaki, S. Uchida, T. Tohyama, and S. Maekawa, *Phys. Rev. Lett.* **77**, 4054 (1996).
- ²¹R. Neudert, M. Knupfer, M.S. Golden, J. Fink, W. Stephan, K. Penc, N. Motoyama, H. Eisaki, and S. Uchida, *Phys. Rev. Lett.* **81**, 657 (1998).
- ²²A.O. Gogolin, A.A. Nersesyan, and A.M. Tsvelik, *Bosonization and Strongly Correlated Systems* (Cambridge University Press, Cambridge, England, 1998).